QCA Circuits for Robust Coplanar Crossing

Sanjukta Bhanja [1], Marco Ottavi [2], Salvatore Pontarelli [3] and Fabrizio Lombardi [2]

[1] Department of Electrical Engineering

University of South Florida,

Tampa, (FL) 33620, USA

Email: bhanja@eng.usf.edu

[2] Department of Electrical and Computer Engineering

Northeastern University,

Boston, (MA) 02115, USA

Email: {mottavi,lombardi}@ece.neu.edu

[3] Dipartimento di Ingegneria Elettronica

Università di Roma "Tor Vergata"

Rome, 00133, Italy

Email: pontarelli@ing.uniroma2.it

Abstract

In this paper, different circuits of Quantum-dot Cellular Automata (QCA) are proposed for the so-called coplanar crossing. Coplanar crossing is one of the most interesting features of QCA because it allows for mono-layered interconnected circuits, whereas CMOS technology needs different levels of metalization. However, the characteristics of the coplanar crossing make it prone to malfunction due to thermal noise or defects. The proposed circuits exploit the majority voting properties of QCA to allow a robust crossing of wires on the Cartesian plane. This is accomplished using enlarged lines and voting. A Bayesian Network (BN) based simulator is utilized for evaluation; results are provided to assess robustness in the presence of cell defects and thermal effects. The BN simulator provides fast and reliable computation of the signal polarization versus normalized temperature. Simulation of the wire crossing circuits at different operating temperatures is provided with respect to defects and a quantitative metric for performance under temperature variations is proposed and assessed.

I. INTRODUCTION

Quantum-dot Cellular Automata (QCA) [16] may overcome some of the limitations of current technologies, while meeting the density foreseen by Moore's Law and the International Technology Roadmap for Semiconductors (ITRS). For manufacturing, molecular QCA implementations have been proposed to allow for room temperature operation; the feature of wire crossing on the same plane (coplanar crossing) provides a significant advantage over CMOS. Coplanar crossing is very important for designing QCA circuits; multi-layer QCA has been proposed [4] as

an alternative technique to route signals, however it still lacks a physical implementation. At design level, algorithms have been proposed to reduce the number of coplanar wire crossings [9]. In QCA circuits, a reliable operation of coplanar crossing is dependent on the temperature of operation. Resilience to temperature variations due to thermal effects is also an important feature to consider for practical applications. A reduction in the probability of generating an erroneous signal is also of concern, hence, robustness must be addressed.

Robustness to thermal effects must consider the repeated estimates of ground (and preferably near-ground) states, along with cell polarization for different designs. This evaluation is presently possible only through a full quantum-mechanical simulation (over time) that is known to be computationally intensive. Tools such as AQUINAS [16] and the coherence vector simulation engine of QCADesigner [17] perform an iterative quantum mechanical simulation (as a self consistent approximation, or SCA) by factorizing the joint wave function over all QCA cells into a product of individual cell wave functions (using the Hartree-Fock approximation). This results in accurate estimates of ground states, cell polarization (or probability of cell state), temporal progress and thermal effects, but also at the expense of a large computational complexity. Other techniques such as QBert [12], Fountain-Excel simulation, nonlinear simulation [14], [17], and digital simulation [17] are faster, but they only estimate the state of the cells; in some cases unfortunately, they may fail to estimate the correct ground state. Also these techniques do not fully estimate the cell polarization or take into account thermal effects. In this paper, we use a Bayesian modeling method that allows to estimate the cell polarization for the ground state and to study the effects of thermal variations and layout defects. As introduced in [1], a Bayesian model makes possible to perform a thermal characterization of coplanar crossing; in the next sections, the Bayesian model is also amenable for simulating the combined effects of layout defects and temperature.

The objective of this paper is to propose and analyze different circuits for QCA coplanar crossing. The coplanar crossing designs that are analyzed in this paper are for two signals orthogonally routed on the same plane using the following circuits: (1) the coplanar crossing of [8], (2) a novel TMR-based coplanar crossing , (3) the so-called thick coplanar crossing of [3]. This paper deals with the robust operation of these three coplanar crossing circuits to thermal variation and in the presence of cell defects; the proposed circuits utilize different features of the majority voting function of QCA circuits to route signals on a Cartesian plane. Also, they utilize different types of QCA cells (rotated and not rotated) and their immediate adjacency. The objective of this analysis is to select the coplanar crossing circuit that offers the highest performance. Finally a simulation on a full adder circuit proves that the use of the proposed crossing designs increases the thermal and defect robustness when applied to a generic circuit.

This paper is organized as follows: Section II provides a brief overview of QCA technology, Section III introduces the Bayesian model used for temperature characterization and Section IV describes the coplanar wire crossing circuits (inclusive of layouts). Section V provides an analysis of the designs with respect to normalized temperature, while Section VI shows the simulation results for defective circuits. Section VII shows the results of the thermal characterization of defective layouts under temperature variations while Section VIII analyzes the thermal and defect robustness of a full adder circuit. Finally, Section IX draws the conclusion of this analysis.

II. Review of QCA

A QCA cell can be viewed as a set of four charge containers or "dots", positioned at the corners of a square. The cell contains two extra mobile electrons which can quantum mechanically tunnel between dots, but not cells. The electrons are forced to the corner positions by Coulomb repulsion. Therefore, electrons have a preferential alignment along one of the two perpendicular cell axes, as shown in Figure 1. The polarization δ [1] measures the extent of this alignment.

If the two extra electrons are completely localized on dots 1 and 3, the polarization is + 1 (binary 1); if they are localized on dots 2 and 4, the polarization is - 1 (binary 0). Tunneling between dots implies that charges may not be not completely localized and consequently, the polarization value can be not integer.
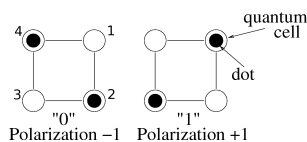

Fig. 1.   QCA cell and polarization states

Unlike conventional logic circuits in which information is transferred by electrical current, QCA operates by the Coulombic interaction that connects the state of one cell to the state of its neighbors. This results in a technology in which information transfer (interconnection) is the same as information transformation (logic manipulation) with low power dissipation [15]. One of the basic logic gates in QCA is the so-called majority voter (MV) with logic function $\text{Maj}(A, B, C) = AB + AC + BC$. MV can be realized by 5 QCA cells, as shown in Figure 2(1b). Logic AND and OR functions can be implemented from the MV by setting an input (the so-called programming or control input) permanently to a "0" or "1" value. The inverter (INV) is the other basic gate in QCA and is shown in Figure 2(1a). The binary wire and inverter chain (as interconnect fabric) are shown in Figure 2(1c)(1d). In VLSI systems, timing is controlled through a reference signal (i.e. the clock), however timing in QCA is accomplished by clocking in four distinct and periodic phases [5] (as shown in Figure 2 (2)). A QCA circuit is partitioned into *serial* (one-dimensional) zones, and each zone is maintained in a phase. Clocking implements quasi adiabatic switching to ensure that the QCA cells reach the lowest energy state (or ground state) during this operation.

III. Bayesian Model

An approximate two-state model of a single QCA cell [16] is utilized. In this model, each cell can be observed to be in one of two possible states, corresponding to logical states 0 and 1. Let the probability of *observing* the $i - th$ QCA cell at state 0, be denoted by $P(X_i = 0)$ or $P_{X_i}(0)$, or simply by $P(x_i)$. Hence for *polarization*, $\delta_{X_i} = P_{X_i}(1) - P_{X_i}(0)$. The joint probability of observing a set of steady-state assignments for the cells is denoted by $P(x_1, \cdots, x_n)$. To reduce the combinatorial complexity of the analysis, the joint wave function must

---

[1]δ refers to polarization as P is used for defining probabilities.
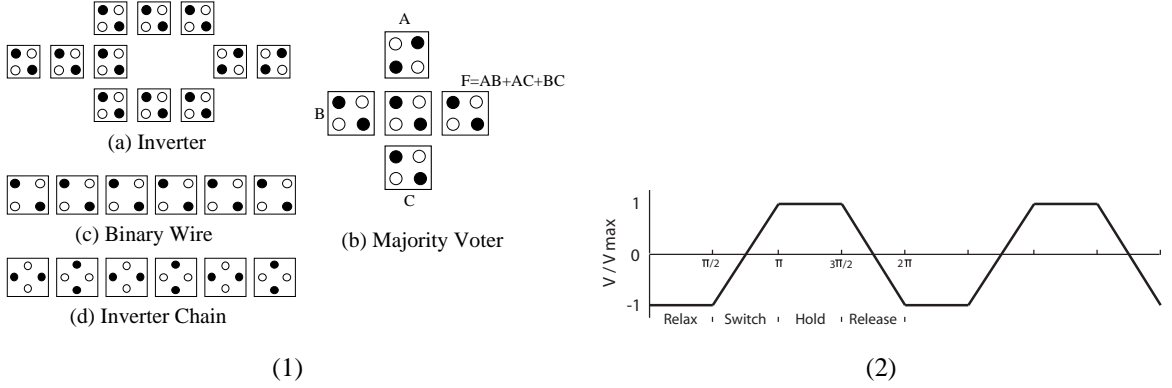
Fig. 2. (1) Basic QCA devices (2) Cmos-Clock-Signal

be considered in terms of the product of the wave function over one or two variables (i.e. the Slater determinants). This corresponds to a factored representation of the wave function (Hartree-Fock approximation) [15] [7]. As an example, consider the linear wire arrangement of 9 QCA cells, shown in Figure 3(a). With no assumption, the joint state probability function can be decomposed into a product of *conditional* probability functions by the repeated use of the property that $P(A, B) = P(A|B)P(B)$ (as shown in Figure 3d).

$$P(x_1, \cdots, x_9) =$$
$$= P(x_9|x_8 \cdots x_1)P(x_8|x_7 \cdots x_1) \cdots P(x_2|x_1)P(x_1)$$

(1)

The *radius of influence* (denoted by r) is defined as the maximum distance (normalized to the cell-to-cell distance) that allows interaction between two cells. If a 2-cell radius ($r = 2$) of influence is considered, then the conditional probability $P(x_i|x_{i-1}, \cdots, x_1)$ can be approximated by $P(x_i|x_{i-1}, x_{i-2})$, and the overall joint probability can be factored as

$$P(x_1, \cdots, x_9) =$$
$$\begin{cases} P(x_9|x_8, x_7)P(x_8|x_7, x_6) \cdots P(x_2|x_1)P(x_1) & r = 2 \\ P(x_9|x_8)P(x_8|x_7) \cdots P(x_2|x_1)P(x_1) & r = 1 \end{cases}$$

A. Inferring Link Structure

The complexity of a Bayesian network representation is dependent on the order of the conditional probabilities, i.e. the maximum number of parents (N_p) for a node. The maximum size of the conditional probability table stored is 2^{N_p+1}; thus, it is important to have a representation with a minimal possible number of parents per node, while preserving all dependencies. For this representation conditional *independencies* that might exist must be used.
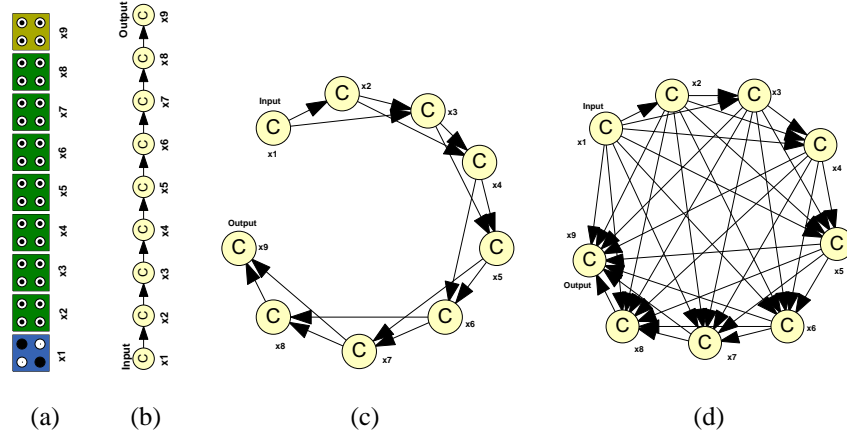
Fig. 3. Bayesian net dependency model (BN) for (a) 9-cell QCA wire with (b) 1-cell radius of influence (c) 2-cell radius of influence, and (d) all cells.

Note that modeling all dependencies is possible by utilizing a complete graph representation; however, it is the independencies that result in a sparse graph representation. It can be shown that all conditional *independencies* among all triple subsets of variables can be captured by a directed acyclic graph (DAG) representation if the links are directed along *causal* directions [13], i.e. a parent should represent the direct causes of its children. Such minimal representations are termed Bayesian networks. A link is directed from node X to node Y, if X is a direct cause of Y. For QCA circuits, there is an inherent causal ordering among cells. Part of the ordering is imposed by the clocking zones. Cells in the previous clock zone are the drivers or the causes of the change in polarization of the current cell. Within each clocking zone, ordering is determined by the direction of propagation of the wave function [16].

Let $Ne(X)$ denote the set of all neighboring cells than can effect a cell, X. It consists of all cell within a pre-specified radius. Let $C(X)$ denote the clocking zone of cell X (as commonly assumed for phased clocking zones in QCA). Let $T(X)$ denote the time for the wave function to propagate from the nodes nearest to the previous clock zone or from the inputs, if X shares the clock with the inputs. Only the relative values of $T(X)$ are important to decide upon the causal ordering of the cells. A breadth first search strategy, outlined in Fig. 4 is employed to decide upon the time ordering, $T(X)$.

The direct causes or parents of a node X are determined based on the inferred causal ordering; this parent set is denoted by $Pa(X)$ and is logically specified as follows.

$$Pa(X) = \{Y | Y \in Ne(X), (C(Y) <_{mod4} C(X)) \vee (T(Y) < T(X))\} \tag{2}$$

The *causes*, and hence the parents, of X are the cells in the previous clocking zone and the cells are nearer to the previous clocking zone than X. The children set, $Ch(X)$, of a node, X, are the neighbor nodes that are not parents, i.e. $Ch(X) = Ne(X)/Pa(X)$.

An important part of a Bayesian network is the conditional probabilities $P(x|pa(X))$, where $pa(X)$ represents the values taken on by the parent set, $Pa(X)$.

```
Variables:
  Q: queue to process cells in a breadth first order
  T(X): each cell, X, has a time tag, T(X), that is initialized to -1
  Count: counter that is incremented at each iteration.
  Clock: to keep track of the clock zone being processed.


1.   Enqueue input cells onto Q
2.   Set time tags of input cells to -2 to denote cells in Q
3.   do repeat
4.       while Q is not empty
5.           X = Dequeue(Q);
6            Clock = Clock(X);
7.           T(X) = Count++;
8.           Ne(X) = Neighbors of X sorted from nearest to farthest
9.           for neighbor, Y,  in Ne(X)
10.              if Y has not been tagged, i.e. T(Y) == -1, and
                    Y is in the same clock zone as X
11.                      Enqueue(Q, Y)
12.                      T(Y) = -2
13.              end if
14.          end for
15.      end while
16.      Enqueue cells onto Q that are adjacent to cells in Clock zone
17.      Set the time tags of these cells to -2;
18.  while (Q is not empty)
```

Fig. 4.   Breadth-first search algorithm to establish the causal order of the QCA cells.

B. Quantification of Conditional Probabilities

In a four-phased clocked design [16],all cells must be placed into the ground state by systolically driving subgroups of cells (all in one clock zone) into their local ground states. So, in this respect the conditional probabilities are the probabilities of the ground states, defined locally over the Markov neighborhood of each cell, i.e. to decide upon the conditional probability of a cell state given the states of the parent nodes, $P(X = 1|Pa(X) = pa(X))$. Hence, all cells within the Markov neighborhood, $Ne(X)$ must be considered. This includes the cells that are the parents in the Bayesian network representation $Pa(X)$ and also the children, $Ch(X)$. The states of these parents are fixed

at the conditioned state assignments $pa(X)$; however, the states of the children are unspecified. As a clocked circuit is modelled (in this circuit the phased clock design keeps the cells at their ground states in each clocking epoch), then the polarization of X and $Ch(X)$ is chosen such that given the parent states, the energy (Hamiltonian) in the local neighborhood is minimized. A quantum mechanical formulation is effectively achieved.

An array of cells can be modeled by considering the cell-level quantum entanglement of the two states and the Coulombic interaction of nearby cells (that is modeled using the Hartee-Fock (HF) approximation [16], [10]). The HF model approximates the joint wave function over all cells by the product of the wave functions over individual cells (actually the sum of permutations of the individual wave functions by their Slater determinant). This allows to characterize the evolution of the individual wave functions. The evolution of the wave function of the cell X in the local neighborhood $Ne(X)$ is of interest.

Let denote the eigenstates of a cell corresponding to the 2-states by $|0\rangle$ and $|1\rangle$. The state at time t, that is referred to as the wave-function and denoted by $|\Psi(t)\rangle$, is a linear combination of these two states, i.e. $|\Psi(t)\rangle = c_0(t)|0\rangle + c_1(t)|1\rangle$. The coefficients are function of time. The expected value of any observable, $\langle \hat{A}(t) \rangle$, can be expressed in terms of the wave function as $\langle \hat{A} \rangle = \langle \Psi(t)|\hat{A}(t)|\Psi(t)\rangle$ or equivalently as $\text{Tr}[\hat{A}(t)|\Psi(t)\rangle\langle\Psi(t)|]$, where Tr denotes the trace operation, $\text{Tr}[\cdots] = \langle 0|\cdots|0\rangle + \langle 1|\cdots|1\rangle$. The term $|\Psi(t)\rangle\langle\Psi(t)|$ is known as the density operator, $\hat{\rho}(t)$. The expected value of an observable of a quantum system can be computed if $\hat{\rho}(t)$ is known.

The entries of the density matrix, $\rho_{ij}(t)$, can be shown to be defined by $c_i(t)c_j^*(t)$ or $\rho(t) = \mathbf{c(t)c(t)}^*$, where $*$ denotes the conjugate transpose operation. The density matrix is Hermitian, i.e. $\rho(t) = \rho(t)^*$; each diagonal term, $\rho_{ii}(t) = |c_i(t)|^2$, represents the *probabilities* of finding the system in state $|i\rangle$. It can be easily shown that $\rho_{00}(t) + \rho_{11}(t) = 1$. These two entries of the density matrix are pertinent to logic modeling; ideally, these probabilities should be zero or one. For QCA device modeling, the *polarization* index (P) is commonly used, i.e. $\rho_{00}(t) - \rho_{11}(t)$ as the difference of the two probabilities in a range between -1 and 1.

The density operator is a function of time, $\hat{\rho}(t)$, and its dynamics is captured by the Loiuville equation or the von Neumann equation, that can be derived from the basic Schrodinger equations to capture the evolution of the wave function over time, $\Psi(t)$.

$$
\begin{aligned}
i\hbar\tfrac{\partial}{\partial t}\rho(t) &= i\hbar\tfrac{\partial}{\partial t}\mathbf{c(t)c(t)}^* \\
&= \mathbf{H}\rho(t) - \rho(t)\mathbf{H}
\end{aligned}
\tag{3}
$$

where $\mathbf{H}$ is a 2 by 2 matrix representing the Hamiltonian of the cell. For QCA cells, it is common to assume only Columbic interaction between cells and use the Hartree-Fock approximation to arrive at the matrix representation of the Hamiltonian given by [16]

$$
\mathbf{H} = \begin{bmatrix} -\tfrac{1}{2}\sum_{i \in Ne(X)} E_k \delta_i f_i & -\gamma \\ -\gamma & \tfrac{1}{2}\sum_{i \in Ne(X)} E_k \delta_i f_i \end{bmatrix}
\tag{4}
$$

where the sums are over the cells in the local neighborhood, $Ne(X)$. E_k is the energy cost of two neighboring cells having opposite polarizations; this is also referred to as the "kink energy". f_i is the geometric factor capturing the electrostatic fall off with distance between cells. δ_i is the polarization of the i-th neighboring cell. The tunneling energy between the two states of a cell, that is controlled by the clocking mechanism, is denoted by γ.

In the presence of inelastic dissipative heat bath coupling (open world), the system moves towards the ground state [16], [10]. At thermal equilibrium, the steady-state density matrix is given by

$$\rho^{ss} = \frac{e^{-\mathbf{H}/kT}}{\text{Tr}[e^{-\mathbf{H}/kT}]} \tag{5}$$

where k is the Boltzman constant and T is the temperature. Of particular interest are the diagonal entries of the density matrix, that express the probabilities of observing the cell in the two states. They are given by

$$
\begin{aligned}
\rho_{11}^{ss} &= \tfrac{1}{2}\left(1 - \tfrac{E}{\Omega}\tanh(\Delta)\right) \\
\rho_{22}^{ss} &= \tfrac{1}{2}\left(1 + \tfrac{E}{\Omega}\tanh(\Delta)\right)
\end{aligned}
\tag{6}
$$

where $E = \tfrac{1}{2}\sum_{i \in Ne(X)} E_k \delta_i f_i$, the total kink energy at the cell, $\Omega = \sqrt{E^2 + \gamma^2}$, the energy term (also known as the Rabi frequency), and $\Delta = \tfrac{\Omega}{kT}$, is the thermal ratio. These probabilities are used for establishing the minimum energy ground state values. This is determined by the eigenvalues of the Hamiltonian (Eq. 4) that are $\pm\Omega$, a function of the kink energy with the neighbors. However, the states (or equivalently, polarization) of only the parents are specified in the conditional probability that we seek. The polarization of the children are unspecified. The children states (or polarization) are chosen such that Ω is maximized i.e. to minimize the ground state energy over all possible ground states of the cell. Thus, the chosen children states are

$$ch^*(X) = \arg\max_{ch(X)} \Omega = \arg\max_{ch(X)} \sum_{i \in (Pa(X) \cup Ch(X))} E_k \delta_i f_i \tag{7}$$

The steady state density matrix diagonal entries (Eq. 6 with these children state assignments are used to decide upon the conditional probabilities in the Bayesian network (BN):

$$
\begin{aligned}
P(X = 0 | pa(X)) &= \rho_{11}^{ss}(pa(X), ch^*(X)) \\
P(X = 1 | pa(X)) &= \rho_{22}^{ss}(pa(X), ch^*(X))
\end{aligned}
\tag{8}
$$

It is presently possible to estimate the polarization and ground state probabilities through a full quantum-mechanical simulation of the system evolution over time, that is known to be computationally intensive. Tools such as AQUINAS [16] and the coherence vector engine of QCADesigner [17] perform an iterative quantum mechanical simulation (self consistent approximation, SCA) by factorizing the joint wave function over all cells into a product of individual cell wave functions exploiting the Hartree-Fock approximation. These approaches obtain accurate results for the computation of ground states, cell polarization (or probability of cell state), temporal progress, and thermal effects, but they are slow. In addition, they cannot estimate the near-ground state configurations, that are important for analyzing the sensitivity of circuits to parametric variations (such as temperature). Other tools such as QBert [12], nonlinear simulation [17], and digital simulation [17] are fast iterative schemes; however, they just estimate the state of the cells and in some cases, some fail to estimate the correct ground state. Moreover, they do not estimate the cell polarization and can not take into account temperature effects. The BN simulator presented in [2] is used in this work because it is is very efficient in terms of computational complexity and its features are well suited to analyze parametric variations in the operation of a circuit. In particular this simulator provides the following features as outcome:

1) The ground state configuration;

2) The polarization of each cell;

3) The probability of the near-ground state (next to the lowest one) to study sensitivity to the most probable erroneous behavior (such as due to variations in operating parameters or defects);

4) The feature of each type of cell (rotated and non-rotated) to ensure robustness in operation;

5) The study of the thermal characteristics of a QCA circuit;

IV. COPLANAR CROSSING CIRCUITS

Coplanar wire crossing is one of the most interesting features of QCA; it allows for the physical intersection of horizontal and vertical QCA wires on the same plane, while retaining logic independence in their values; the vertical wire is implemented by rotating the QCA-cells at 45 degrees i.e. by means of an inverter chain. The feature of this structure is that the information along the vertical wire does not interact with the horizontal, wire. Crossing is obtained by *interrupting* either the horizontal, or the vertical wire; these interruptions are hereafter also referred to as *cuts*. Switching of the signals is accomplished by the four phased clock through the release phase.

As in previous papers in the technical literature, layouts are considered to be in a single clocking zone. The outputs are evaluated when the ground state is attained by quasi adiabatic switching. A different approach [6] proposes the vertical and horizontal waves alternatively passing through an intersection. While this approach has the interesting feature of exploiting the intrinsically pipelined behavior of QCA, crossings in a single clocking zone require less area and a simple clocking circuitry.

A set of three layouts for the coplanar crossing analogous to that introduced in [1] is hereafter analyzed.

1) *Normal crossing: this is based on the orientation of the cells.*

2) *TMR crossing: this is based on the voting nature in the QCA layout.*

3) *Thick crossing: this is based on the interaction among cells in an enlarged wire.*

For normal crossing, the cell orientation is interrupted on the central cell of either the horizontal (A line), or vertical line (B line). For the other two circuits, the cell orientation is interrupted on the horizontal (A line), or vertical line (B line).

A. Normal

The normal coplanar crossing circuit can have two arrangements (shown in Figures 5 and 6) as corresponding to the employed cut. This circuit has been proposed in [8]; it has been shown that an horizontal wire (with input A and output $Aout$) can be crossed with a vertical inverter chain (with input B and output $Bout$) with no interference among wires.

These arrangements differ by the orientation of the cell at the crossing point: Xa in Figure 5 (a) has the central cell rotated by 45 degrees, Xb in Figures 6 (a) has a non-rotated cell. Figures 5 (b) and 6 (b) show the BN for analyzing these two arrangements. Note that only the BN shown in Figure 5 (b) reports the actual number of
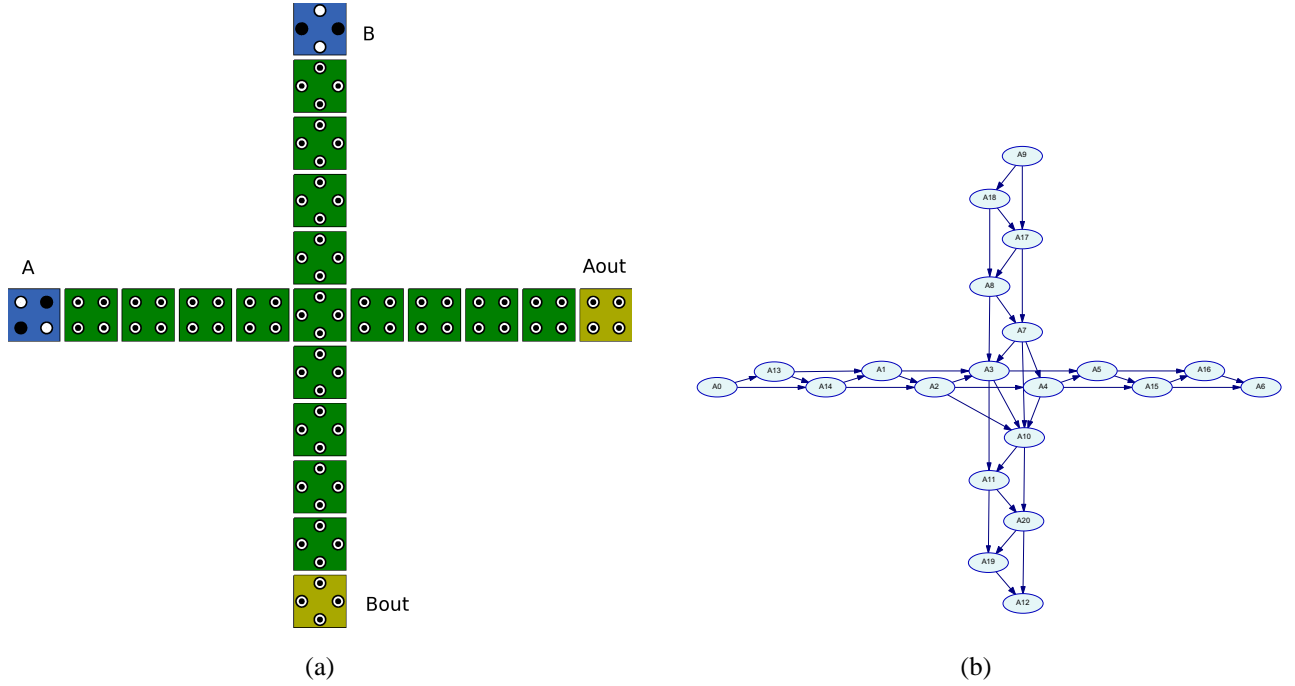
Fig. 5.   Normal crossing with rotated central cell (Xa) (a) Layout (b) BN with 2-cell radius of influence.

connections which account for a radius of influence of two; hereafter in this paper, all BNs are simplified for improved readability of the figures.

B. TMR

A simple approach for implementing robust crossing in QCA is to take advantage of the inherent voting characteristic of this technology. The QCA wire is split through fanout, crossed and then re-converged and voted by a MV which performs a TMR voting function of the signals.

Two types of arrangement for the TMR based coplanar crossing circuit are proposed:

1) 3-to-1 TMR;

2) 3-to-3 TMR.

In the 3-to-1 TMR shown in Figure 7 and associated BN, voting occurs along the direction on which the cell rotation is interrupted, thus producing two different arrangements TMR_Xa for voting the A line and TMR_Xb for voting the B line (shown in Figure 7) .

If both wires are split and reconverged, the more complex 3-to-3 (triple) TMR (as shown in Figure 8 with corresponding BN) is applicable. The triple TMR has also two arrangements: double_TMR Xa (Figure 8) for the interrupted A line direction, and double_TMR Xb for the interrupted B line direction. The 3-to-3 TMR utilizes a larger number of cells (92 versus 41) than the 3-to-1 TMR.
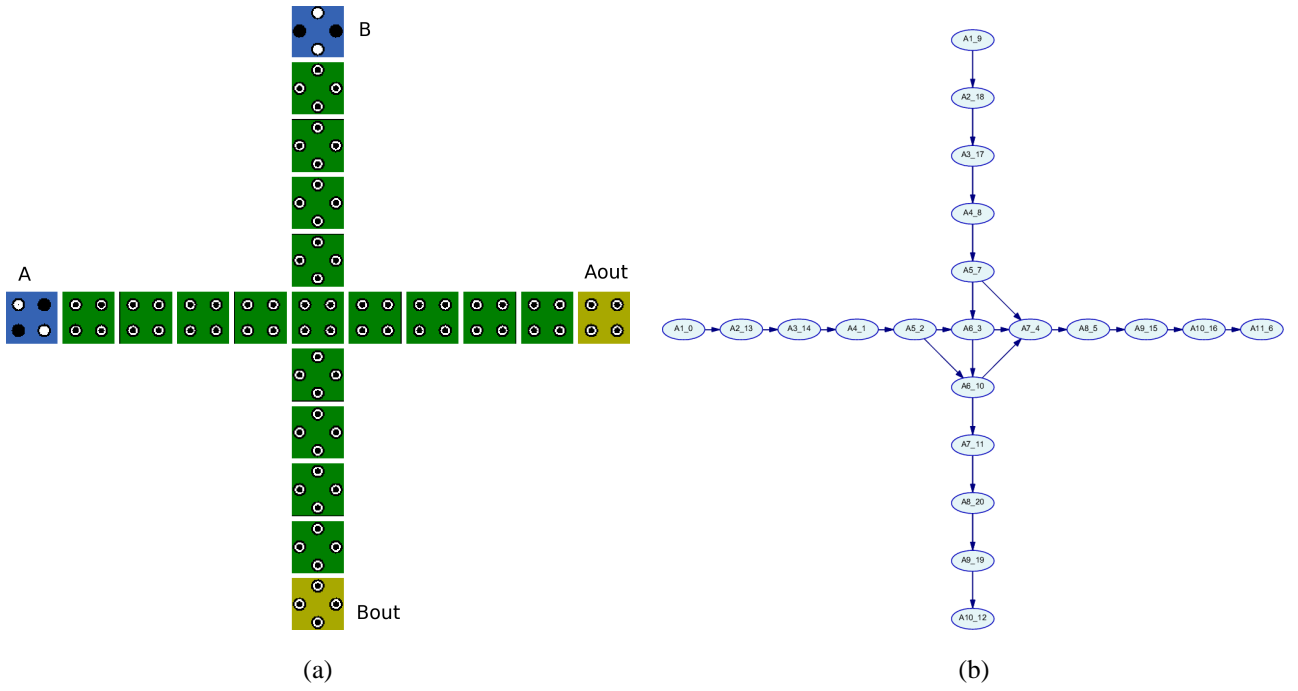
Fig. 6. Normal crossing with rotated central cell (Xb) (a) Layout (b) BN with 2-cell radius of influence.
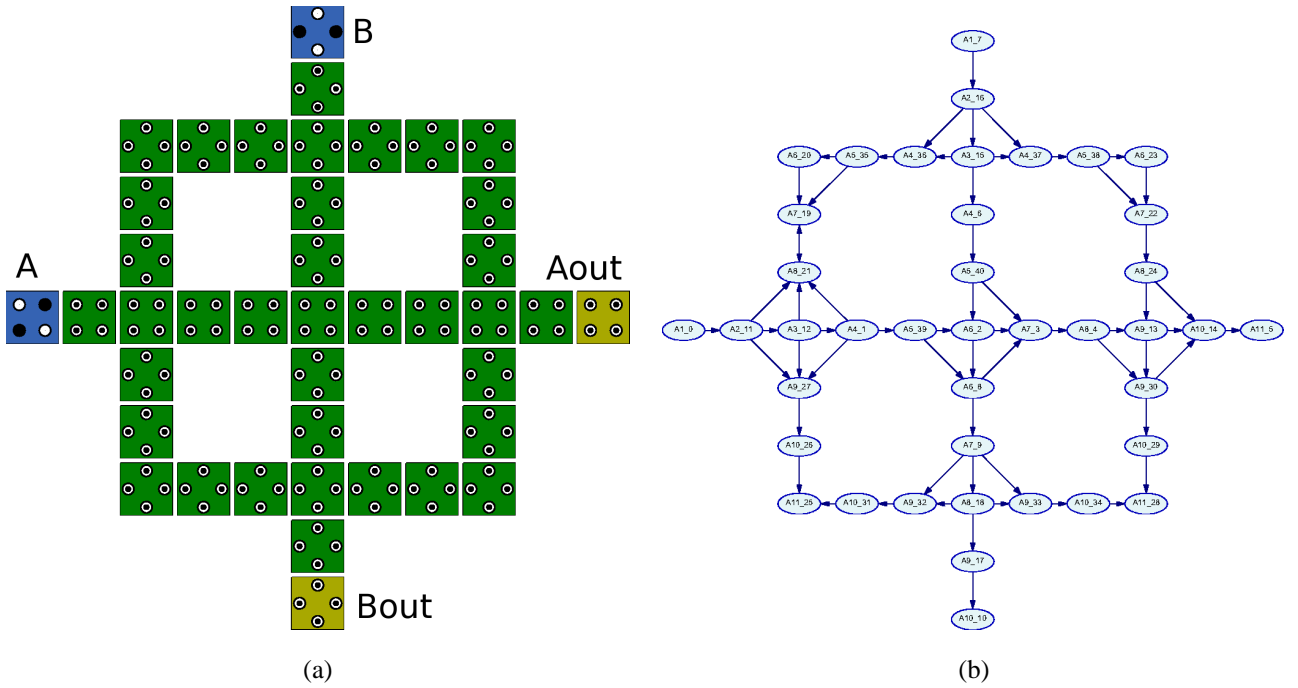

Fig. 7. 3x1 TMR crossing with non rotated central cell (TMRXb voting on the B line) (a) Layout (b) BN with 2-cell radius of influence.
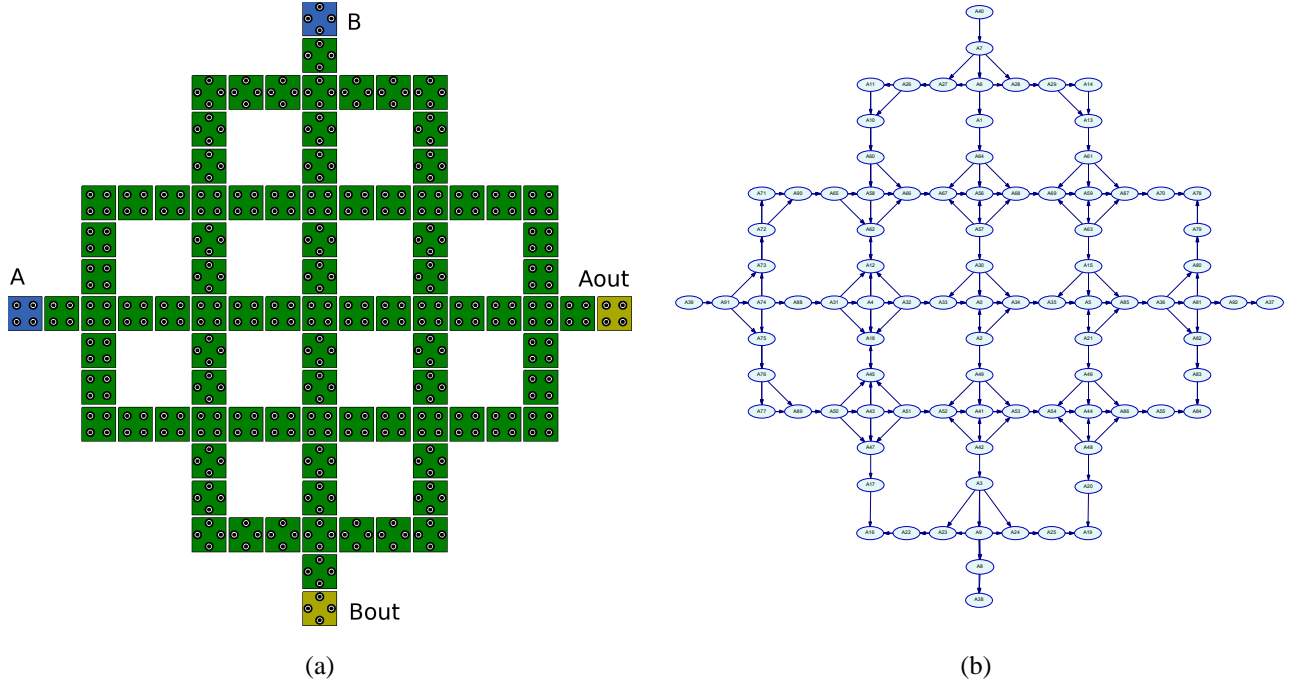
Fig. 8.   3 x 3 TMR crossing with rotated central cell (a) Layout (b) BN with 2-cell radius of influence.

C. Thick

A coplanar crossing circuit that is still based on TMR voting, has been proposed in [3] and is hereafter referred to as thick crossing. Differently from TMR, in thick crossing the fanout of the three wires generates a "thick" wire that has a width of three cells; crossing between wires is performed by interrupting the thick wire with a single wire whose cells are rotated with respect to the thick wire. Figures 9 and 10 show these arrangements together with the corresponding BN for horizontal and vertical crossings. A thick circuit requires 37 QCA cells.

V. TEMPERATURE CHARACTERIZATION

This section presents the simulation results using the Bayesian network of the proposed coplanar crossing circuits with respect to temperature. All plots start from the correct (expected) value of the output; this output value tends to 0 when the normalized temperature tends to one, i.e. when the temperature is such that $kT \simeq E_k$ (the thermal energy is equal to the kink energy) and the two extra electrons are delocalized. The increase in temperature has different effects on the layouts, therefore allowing to define a metric. Figures 12, 13, 14 and 15 show the output value versus temperature for the previously introduced circuit arrangements when considering the exhaustive combinations of the A, B inputs *i.e.* $(0, 0)$ $(1, 0)$ $(0, 1)$ and $(1, 1)$ respectively. The plots show the robustness of the proposed designs with respect to a temperature increase: a steep slope at the output to reach the zero polarization accounts for an inefficient temperature solution, while a smooth slope shows a good temperature performance. A quantitative metric for evaluating the performance of the different arrangements is also introduced by taking into account the increase
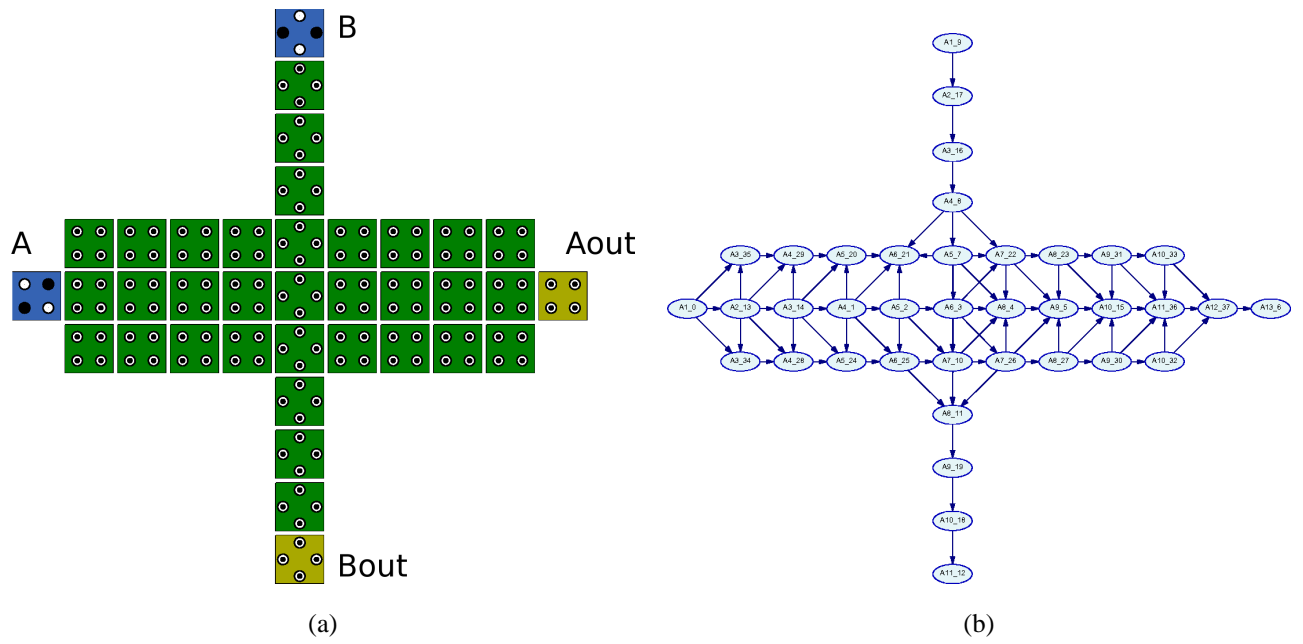
Fig. 9.   Thick horizontal crossing (a) Layout (b) BN with 2-cell radius of influence.
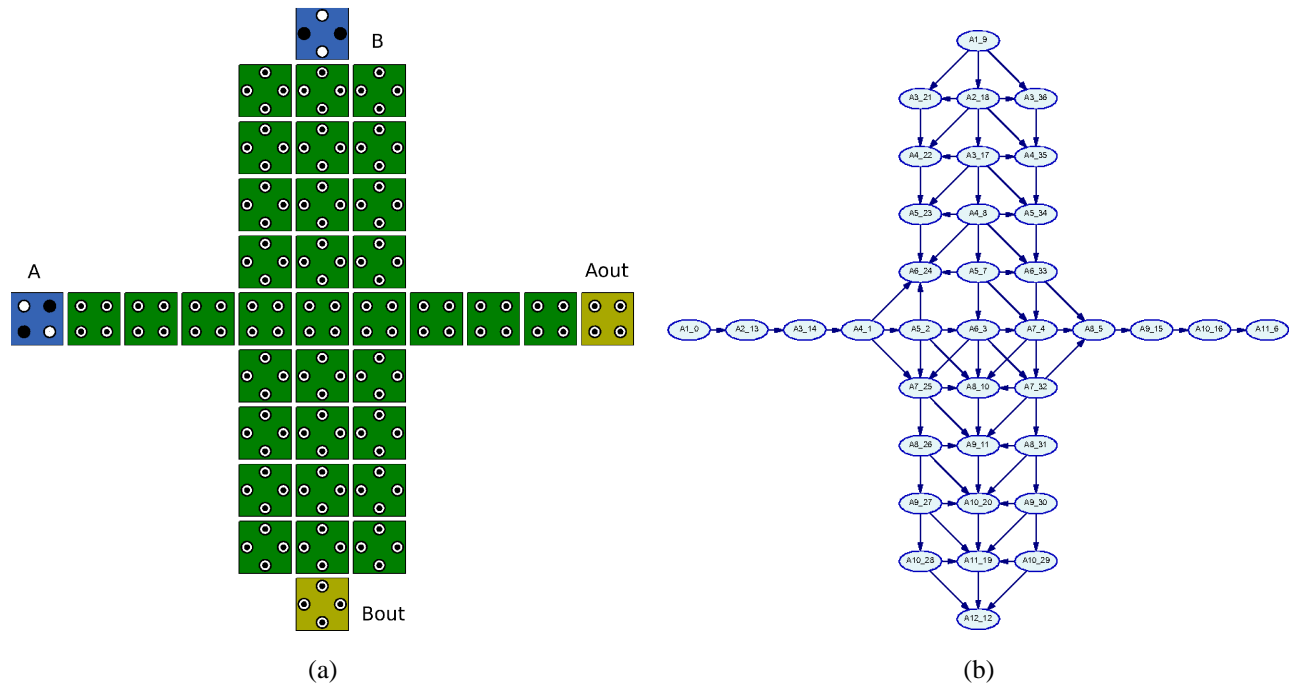

Fig. 10.   Thick vertical crossing (a) Layout (b) BN with 2-cell radius of influence.

of normalized temperature for a drop in output polarization from 90 % to 10% of the nominal value. This metric is referred to as Thermal robustness (Th) and is defined as

$$Th = \Delta T_{\Delta P_{90-10}}$$

Tables I and II report the Th computed for $Aout$ and $Bout$ respectively for the considered coplanar crossing circuits; a higher value accounts for better performance.

A	B	Xa	Xb	TMRXa	TMRXb	dblTMRXa	dblTMRXb	ThickXa	ThickXb	Average
0	0	0.355	0.383	0.429	0.383	0.263	0.35	0.457	0.383	0.375
0	1	0.355	0.383	0.429	0.383	0.263	0.35	0.457	0.383	0.375
1	0	0.355	0.383	0.429	0.383	0.263	0.35	0.457	0.383	0.375
1	1	0.355	0.383	0.429	0.383	0.263	0.35	0.457	0.383	0.375

TABLE I

THERMAL ROBUSTNESS OF AOUT FOR THE DIFFERENT CIRCUITS

A	B	Xa	Xb	TMRXa	TMRXb	dblTMRXa	dblTMRXb	ThickXa	ThickXb	Average
0	0	0.543	0.474	0.543	0.54	0.46	0.33	0.543	0.679	0.514
0	1	0.543	0.474	0.543	0.54	0.46	0.33	0.543	0.679	0.514
1	0	0.543	0.474	0.543	0.54	0.46	0.33	0.543	0.679	0.514
1	1	0.543	0.474	0.543	0.54	0.46	0.33	0.543	0.679	0.514

TABLE II

THERMAL ROBUSTNESS OF BOUT FOR THE DIFFERENT CIRCUITS

The following observation can be drawn from analyzing the plots and tables :

1) In all circuit arrangements, thermal robustness is not affected by the input values, $i.e.$ there is no relation between polarization levels for boolean states and temperature;

2) In all circuit arrangements, the outputs along the uninterrupted direction behave in a similar fashion: for example, in the A direction ThickXb, Xb and TMRXb result in the same Th, because there is no interrupted wire in such direction.

3) The double TMR layout has always the lowest performance along the interrupted direction $i.e.$ dblTMRXa has the lowest Th value in Table I, while dblTMRXb has the lowest Th value in Table II.

4) Thick crossings have always the highest performance along the interrupted direction.

5) Cuts reduce performance, for example double TMRXa has a lower performance than TMRXa.

In general, the Th of $Bout$ is higher than $Aout$ for the same circuit design. This is also applicable if "uncut" circuit arrangements are compared. For example, in Table I, $Aout$ for Xb is 0.383, while in Table II, $Bout$ for Xa is 0.543. The last observation can be explained as follows. The kink energy between two cells is determined by
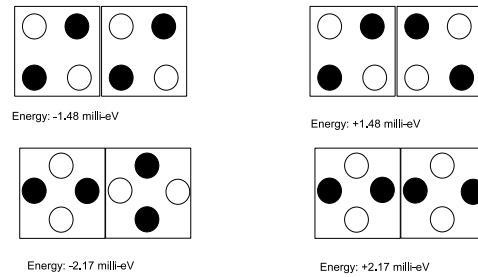
Fig. 11. Configuration energies for normal (top row) and rotated (bottom row) cells. (the lowest energy configurations on the left, the highest energy configurations on the right)

the difference in energy between the higher and the lower energy configurations. Assume two possible states for each cell; then the two possible energy configurations for two cells are shown in Figure 11.

The energy of each configuration is computed by summing the Coulomb energies between the dots in the cells:

$$E_{12} = \sum_{i=1}^{4} \sum_{j=1}^{4} \frac{q_{1i}q_{2i}}{4\pi\epsilon\epsilon_r} \frac{1}{d_{ij}} \tag{9}$$

The charge at the $i - th$ dot of the first cell is denoted by q_{1i}, and the distance between the $i - th$ dot in the first cell and the $j - th$ dot in the second cell is denoted by d_{ij}. On the assumption that there exists a $-1/2q$ charge at each black dot and $+1/2q$ at the white dots, the overall charge of a cell is zero. The kink energy for the normal cell is 2.96 milli eV, while the energy of the rotated cell is higher at 4.34 milli eV. The difference in kink energy is due to the distance between the dots for the two cell types. The distance between two dots in a normal cell is greater than for a rotated cell. Therefore, this suggests that a rotated cell is thermally more stable than a non-rotated one.

VI. Single Defect Characterization

In this section, the coplanar crossing circuits are analyzed with respect to the occurrence of a single missing cell defect. It has been shown in [11] that missing cell placement (as defects) contribute to the almost totality of the logic faults occurring in molecular QCA circuits. Results have been obtained by modifying the Bayesian networks of the coplanar crossing circuits to simulate the absence of cells and record the logic faults due to these defects. Each circuit has been simulated for all possible single missing cell defects under the exhaustive combinations of inputs and at T=10 K (with a Normalized Temperature ratio (kT/Ek)= 0.198), i.e. the highest value (as found previously) prior to the steep drop in performance.

An example of the different effects of QCA cells is shown in Figure 16 in which the case of the polarization of the outputs A and B for inputs $1, 1$ is provided for TMRXahor. The data in Figure 16 shows that the effects of a fault are (a) a strong and mild lack of polarization and (b) a strong and mild inversion at the outputs.
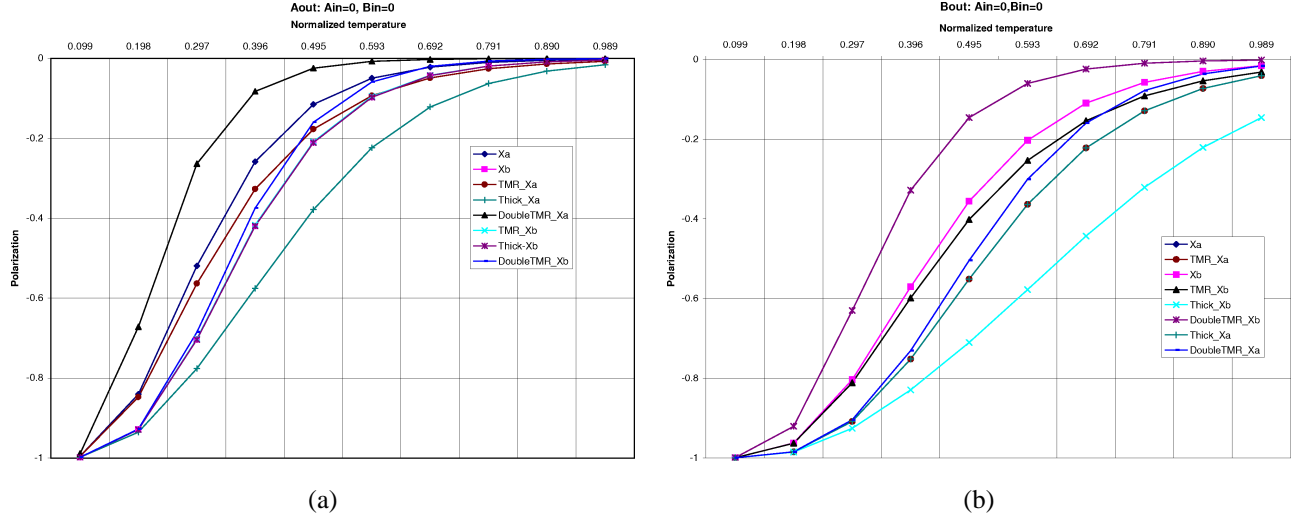
Fig. 12. Output polarization vs normalized temperature for A=0 B=0 (a) $Aout$ (b) $Bout$
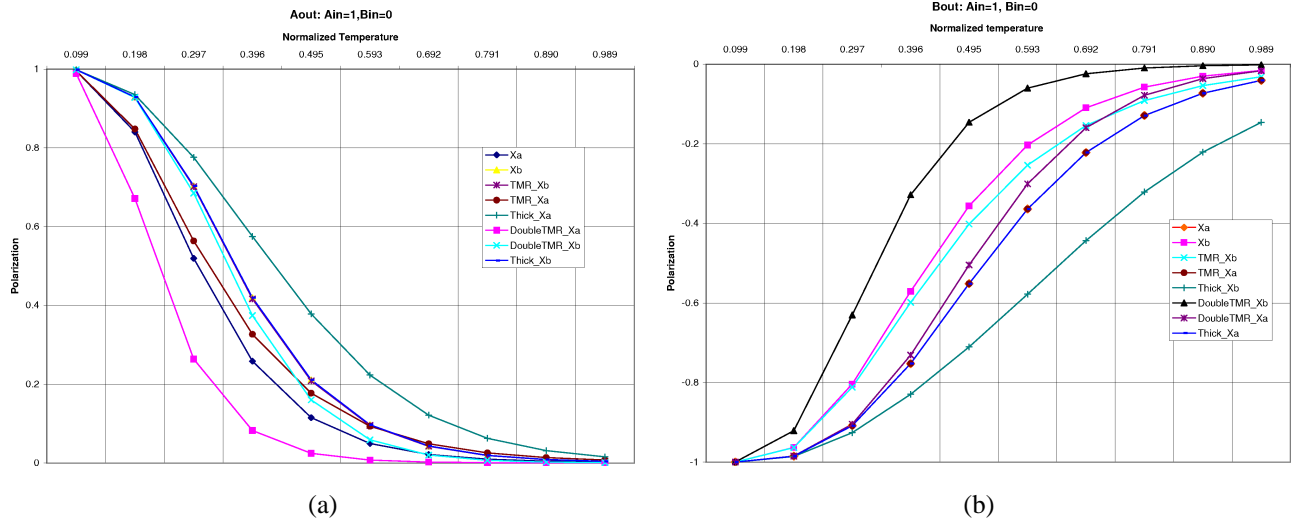

Fig. 13. Output polarization vs normalized temperature for A=1 B=0 (a) $Aout$ (b) $Bout$

Table III reports the results of simulation for all circuit arrangements; the incorrect outputs are either inverted or undetermined (when the polarization is under the threshold of uncertainty given by 0.1). In table III, the results are specified by the number of defective cells resulting in faults on the outputs for each proposed crossing layout.

From the analysis of the simulation results of table III it is evident that as expected, inversion always happens in the B direction (as corresponding to an inverter chain). Moreover, the following conclusions can be drawn.

1) Faults appear at the output independently of the values of the inputs, thus a fault can be detected by any test vector.

2) ThickXb shows the highest performance with respect to a single missing cell defect.
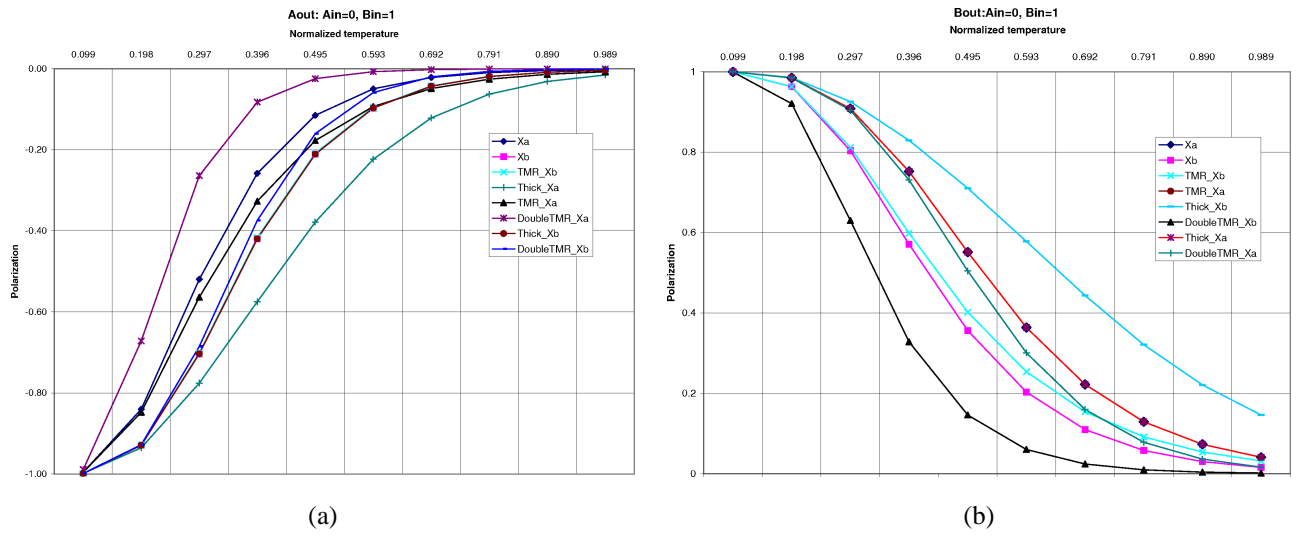
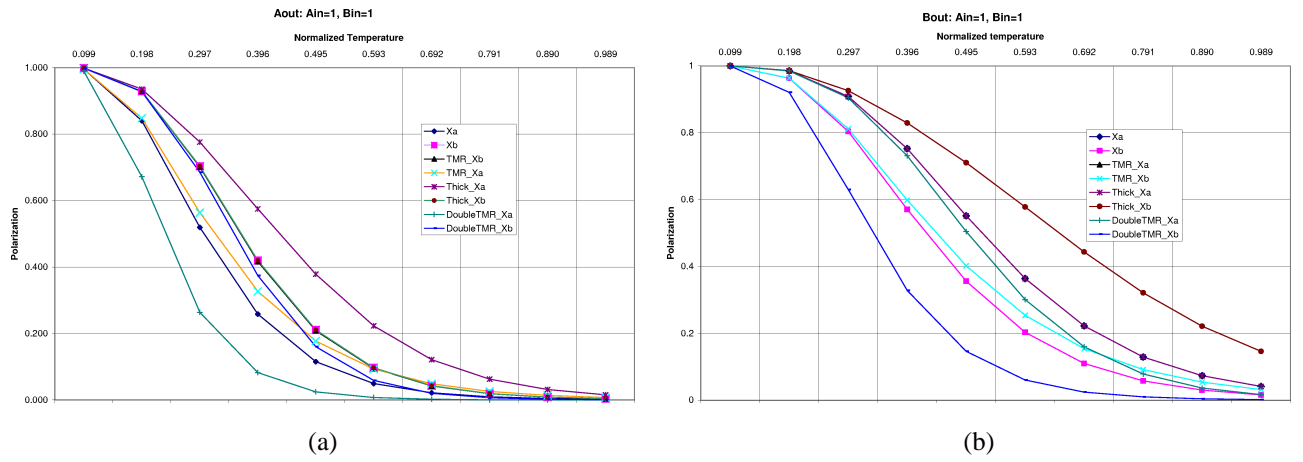Fig. 14. Output polarization vs normalized temperature for *A*=0 *B*=1 (a) *Aout* (b) *Bout*

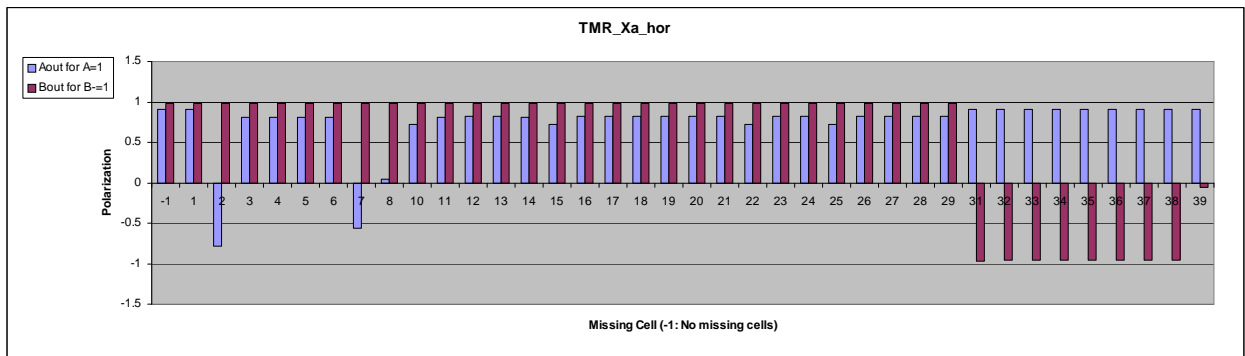Fig. 15. Output polarization vs normalized temperature for *A*=1 *B*=1 (a) *Aout* (b) *Bout*

Fig. 16. TMRXahor

Circuit	Number of cells	Ain=0 Bin=0		Ain=1 Bin=0		Ain=0 Bin=1		Ain=1 Bin=1	
		Inversion	Undet.	Inversion	Undet.	Inversion	Undet.	Inversion	Undet.
Xa	17	8	6	8	6	8	6	8	6
Xb	17	3	6	3	6	3	6	3	6
TMRXaHor	37	4	8	4	8	4	8	4	8
TMRXbHor	37	1	4	1	4	1	4	1	4
ThickXa	35	10	2	10	2	10	2	10	2
ThickXb	35	1	2	1	2	1	2	1	2

TABLE III

DEFECT EFFECTS FOR THE DIFFERENT CIRCUITS

3) Xa shows the lowest performance with respect to a single missing cell defect.

As faults are independent of the values of the inputs, the results are shown in Table IV. The percentages of occurrence for each of the two types of fault are computed as the number of single missing cells over the total number of cells that cause the fault. Also the total percentage of single missing cells causing any type of fault is reported as the sum of the percentage of occurrence of any of the two faults.

Circuit	Fault Occurrence (%)		
	Inversion	Undetermined	Total
Xa	47.1	35.3	82.4
Xb	17.6	35.3	52.9
TMRXaHor	10.8	21.6	32.4
TMRXbHor	2.7	10.8	13.5
ThickXa	28.6	5.7	34.3
ThickXb	2.9	5.7	8.6

TABLE IV

FAULT PERCENTAGES FOR CIRCUITS

The results reported in Table IV show that the coplanar crossing circuits that present the highest resilience to defects, are ThickXb and TMRXbHor.

VII. THERMAL CHARACTERIZATION OF DEFECTIVE CIRCUITS

In the previous sections, defect free circuits with respect to temperature and at a given temperature have been evaluated. In this section, the circuits that have shown the highest resilience to defects are considered further to assess whether the presence of a defect increases the loss of correct polarization at the outputs with an increase of temperature.

The analysis has been performed on the circuits that in the previous section have shown the highest performance, i.e. ThickXb and TMRXbHor. Figure 17 shows the simulation results; as observed previously, the values of the
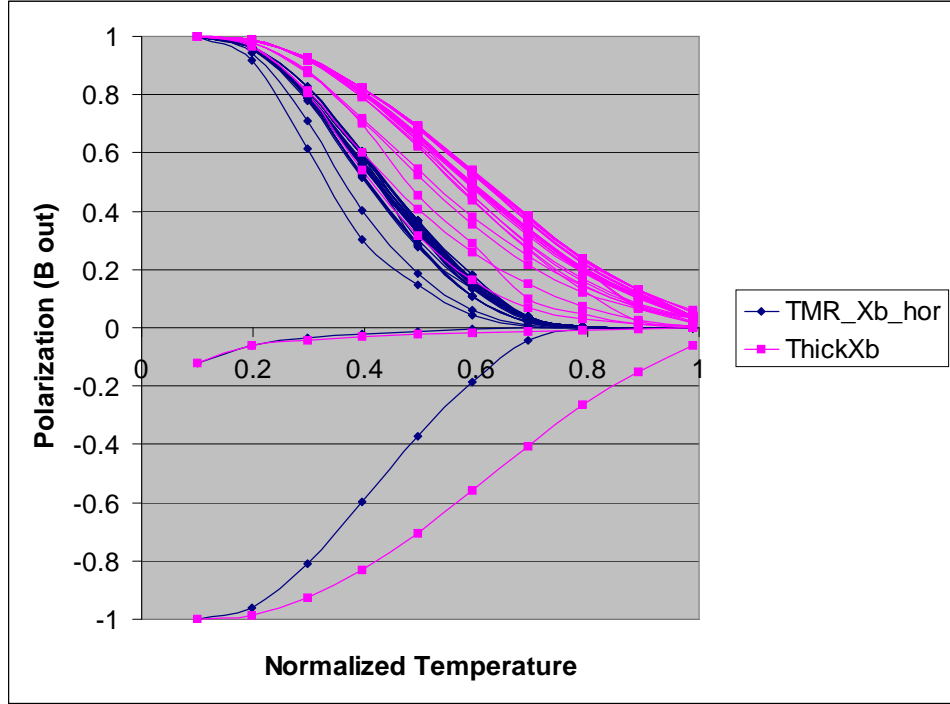
Fig. 17. Polarization vs Temperature for different defects

inputs have no effect, so the results show no inversion when positive (upper half of the figure) and inversion when negative (lower half of the figure). Therefore, the following conclusions can be drawn:

1) Both circuits present two inversions;

2) ThickXb has in almost all cases a better thermal robustness than TMRXb;

The last result and the assumption of randomly distributed defects imply that ThickXb should be preferred as coplanar crossing circuit because on average its thermal robustness is better than TMRXb. To better understand the behavior of these circuits in the presence of defects and resulting faults, the Thermal robustness (Th) (as defined in Section V) has been computed for each simulated defect. The minimum, maximum and median values of Th for the defective circuits has been reported in Tables V and VI. Even if the selected circuits have a good thermal robustness for almost all simulated defects, those defects that produce as fault an inverted value at the outputs, are serious, because the inversion appears also at low temperature. The erroneous outputs appear across the whole temperature range and therefore for these defects, thermal robustness is not fully accounted. The values reported in the tables are computed only for the non inverting defects and the range of Th can be used to provide a quantitative comparison of the robustness of ThickXb and TMRXb.

Tables V and VI show that on the interrupted direction, both circuits behave in a similar manner for the A

A	B	TMRXb			ThickXb		
		Minimum	Median	Maximum	Minimum	Median	Maximum
0	0	0.146	0.268	0.347	0.192	0.257	0.280
0	1	0.147	0.267	0.291	0.192	0.259	0.280
1	0	0.147	0.280	0.347	0.192	0.259	0.279
1	1	0.146	0.265	0.280	0.192	0.251	0.280

TABLE V

THERMAL ROBUSTNESS FOR $Aout$ IN PRESENCE OF DEFECTS

A	B	TMRXb			ThickXb		
		Minimum	Median	Maximum	Minimum	Median	Maximum
0	0	0.307	0.337	0.350	0.3578	0.563	0.602
0	1	0.297	0.336	0.349	0.358	0.563	0.602
1	0	0.298	0.337	0.349	0.358	0.563	0.602
1	1	0.307	0.337	0.349	0.358	0.563	0.602

TABLE VI

THERMAL ROBUSTNESS FOR $Bout$ IN PRESENCE OF DEFECTS

direction, even though ThickXb shows a higher minimum value; for the B direction ThickXb outperforms the TMR circuit. The smallest value of ThickXb is higher than the highest value of TMRXb, corresponding to a better behavior for all possible missing cell defects.

VIII. PERFORMANCE ANALYSIS ON A FULL ADDER

In this section a full adder circuit is analyzed when using the proposed arrangements for the coplanar crossing. Figure 18 shows as an example three of the layouts using Xb TMRXb and ThickXb respectively.

The results of the temperature analysis in Figures 20 and 19 show that ThickXb and ThickXa have the best performance, although the difference between them is less due to the fault masking induced by the inherent signal regeneration of the cell-to-cell non-linear response of QCA. These results are closely dependent on the considered layout and that are not fully applicable in general as when considering the coplanar crossing as a stand-alone device.

The single defect characterization for a full adder using the coplanar crossings Xa TMRXa ThickXa TMRXb ThickXb is reported in table VII.

As done previously for each of the single crossing layouts the simulations were performed after injecting a single missing cell on the layout of the full adder. The targets of the defects were only the coplanar crossings and the number of simulations has been such that every single cell defect on all the coplanar crossings has been injected and its effects simulated and evaluated at the sum and carry outputs. We report the number of faults that generated error in sum outputs in columns 2-5 in Table VII for each cross-wire design for four of the input combinations. For symmetry, results on the other four inputs are not reported. Note that a fault can generate error in sum for more
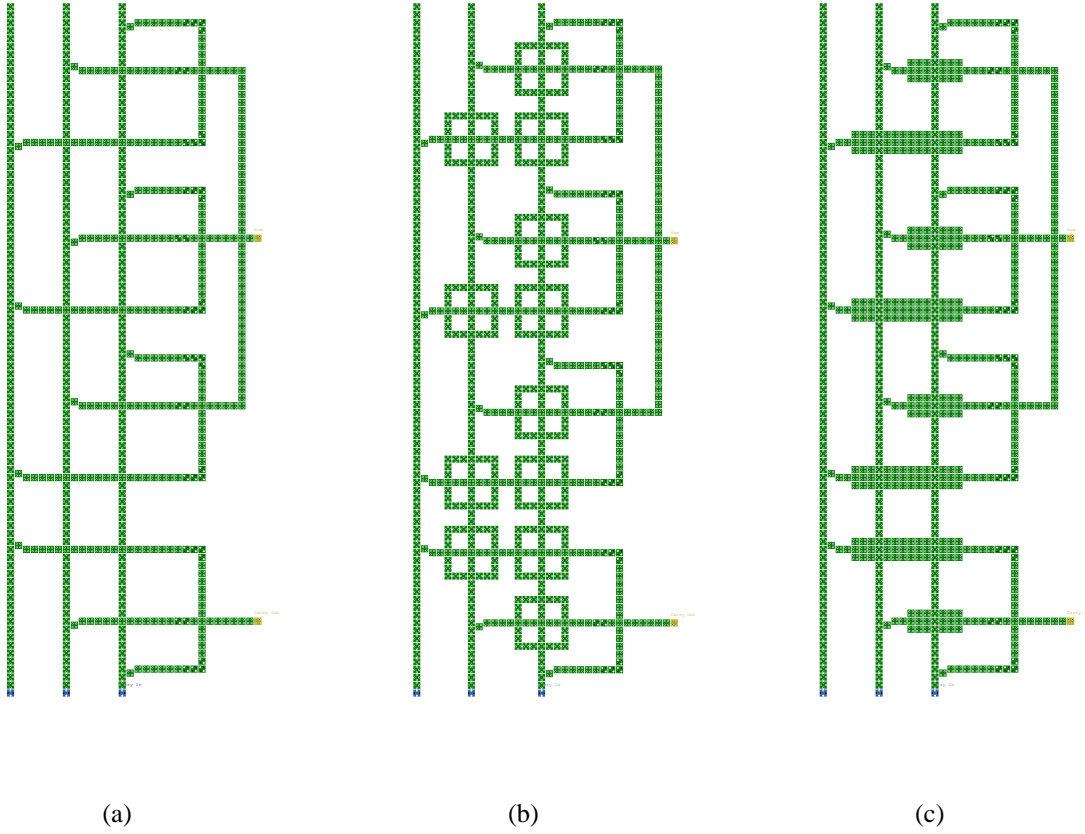
(a)   (b)   (c)

Fig. 18.   Full adder (a) Xb crossings (b) TMRXb crossings (c) ThickXb crossings.

Crosswire Designs	Number of cells	Sum output (Inversions) for inputs				Carry output (Inversions) for inputs			
		"0,0,0"	"0,0,1"	"0,1,0"	"0,1,1"	"0,0,0"	"0,0,1"	"0,1,0"	"0,1,1"
Xa	172	41	61	72	69	2	10	12	1
TMRXa	402	52	80	93	89	0	12	13	3
ThickXa	252	18	42	47	58	0	21	19	5
Xb	180	37	62	82	64	0	0	0	0
TMRXb	396	6	14	20	18	0	0	2	0
ThickXb	252	0	0	0	0	0	0	0	0

TABLE VII

FULL ADDER: FAULT INJECTION OF SINGLE MISSING CELL
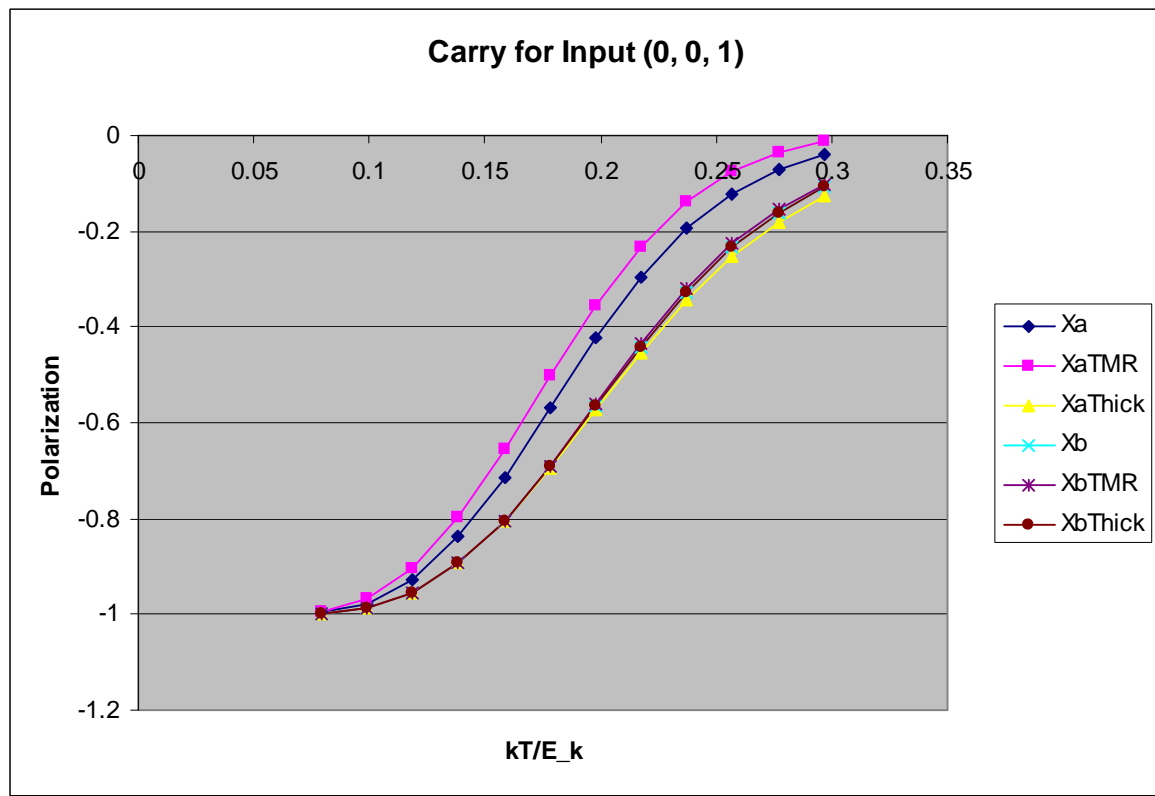
Carry for Input (0, 0, 1)

Fig. 19.   Full Adder: Thermal performances on the carry output

than one input combinations. The same is also reported for the carry outputs in column 6-10 in Table VII.

As could be expected, Table VII shows that Thick crossings especially ThickXb provides the best results in terms of resilience to the occurrence of a single defect.

In Table VIII shows the single missing cell faults (in column 2) that did not generate any error in both outputs sum and carry for all eight input combinations and in column 3 we report the faults that generated at least one output error for at least one input. Fault occurrence percentage is then computed.

We provide the system perspective of both thermal and defect studies however, we believe that relative merits of the various implementation of cross-wires is more meaningful considering them as stand-alone but system analysis would help study various masking effects offered by the layouts.

IX. CONCLUSION

This paper has analyzed the robustness and thermal performance of different circuits for coplanar crossing in Quantum-dot Cellular Automata (QCA). Resilience to temperature and to missing cell defects has been treated in detail. The use of a Bayesian Network (BN) simulator has allowed for fast and reliable computation of the thermal properties of these circuits. The BN simulator is useful for studying the near-ground state (as related to the error probability) and the thermal characterization of QCA circuits. In this paper, it has been shown that in all circuits
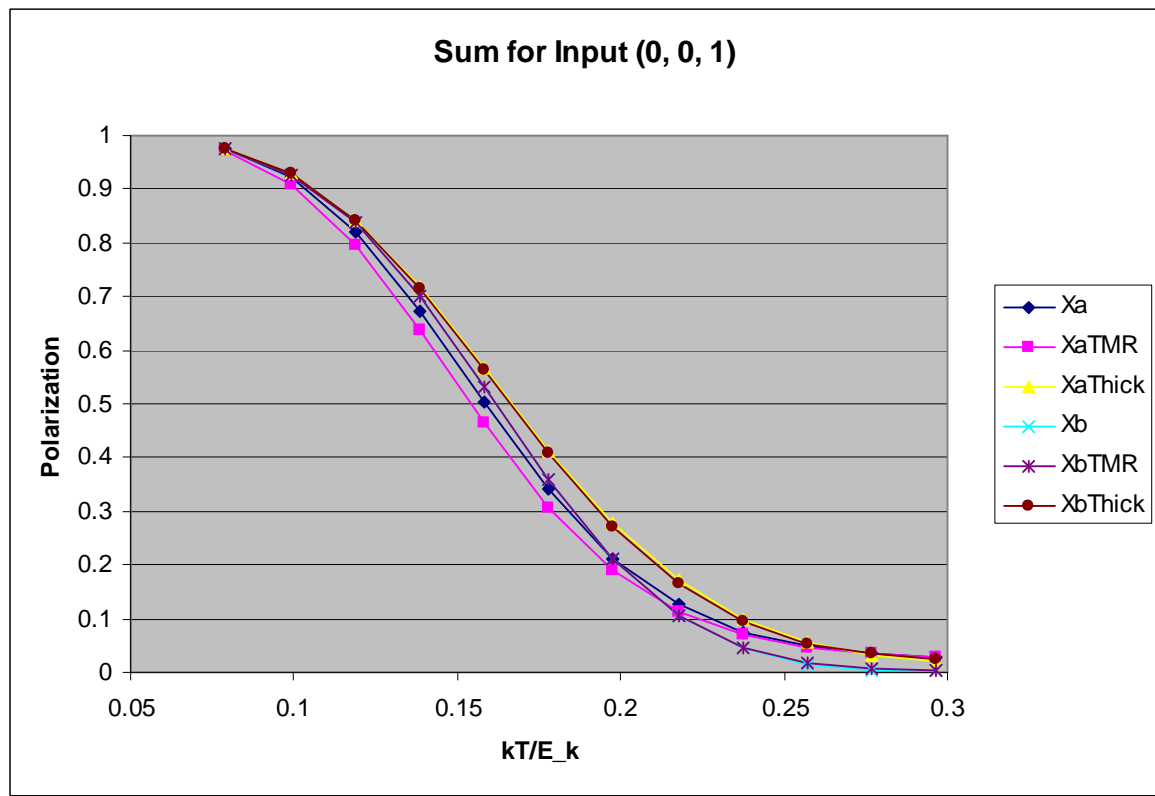
Fig. 20. Full Adder: Thermal performances on the Sum output

and related configurations for the two directions of signal flow, thermal robustness is not affected by input values; moreover, the use of the so-called thick crossing circuit accounts for the highest resilience to temperature. From the simulation results it has been shown and then proved that rotated cells are thermally more stable than non-rotated ones. A missing cell defect model has been evaluated for the coplanar crossing to select the circuit with the highest performance for thermal robustness. Simulation has shown that that a thick crossing circuit is very robust also in presence of defects and related logic faults. Finally a simulation on a full adder circuit has proved that the use of thick crossing increases the thermal and defect robustness.

REFERENCES

[1] S. Bhanja, M. Ottavi, S. Pontarelli, and F. Lombardi. Novel designs for thermally robust coplanar crossing in qca. *IEEE Design and Testing in Europe (to appear)*, 2006.

[2] S. Bhanja, S.; Sarkar. Graphical probabilistic inference for ground state and near-ground state computing in qca circuits. In *IEEE Conference on Nanotechnology*, July 2005.

[3] A. Fijany, N. Toomarian, and K. Modarress. Block qca fault-tolerant logic gates. Technical report, Jet Propulsion Laboratory, California, 2003.

[4] A. Gin, P. D. Tougaw, and S. Williams. An alternative geometry for quantum-dot cellular automata. *J. Appl. Phys.*, 85(12):8281–8286, June 1999.

Designs	"Correct"	"Incorrect"	"Total faults"	Fault Detected %
Xa	77	95	172	55
TMRXa	279	123	402	31
ThickXa	144	108	252	43
Xb	98	82	180	46
TMRXb	370	26	396	7
ThickXb	252	0	252	0

TABLE VIII

PERCENTAGE OF SINGLE MISSING CELL FAULTS IN THE CROSSWIRE DESIGNS THAT ARE DETECTED IN THE SUM AND CARRY OUTTPUTS.

[5] K. Hennessy and C. Lent. Clocking of molecular quantum-dot cellular automata. *Journal of Vacuum Science and Technology*, 19(B):1752–1755, 2001.

[6] C. Lent. Molecular quantum-dot cellular automata. *Seminar*, May 2004.

[7] C. Lent and P. Tougaw. Lines of interacting quantum-dot cells - a binary wire. *Journal of Applied Physics*, 74:6227–6233, 1993.

[8] C. Lent and P. Tougaw. A device architecture for computing with quantum dots. *Proceedings of the IEEE*, 85(4):541–557, April 1997.

[9] S. K. Lim, R. Ravichandran, and M. Niemier. Partitioning and placement for buildable qca circuits. *J. Emerg. Technol. Comput. Syst.*, 1(1):50–72, 2005.

[10] G. Mahler and V. A. Weberruss. *Quantum Networks: Dynamics of Open Nanostructures*. Springer Verlag, 1998.

[11] M. Momenzadeh, M. Ottavi, and F. Lombardi. Modeling qca defects at molecular-level in combinational circuits. *IEEE International Symposium on Defect and Fault Tolerance in VLSI Systems DFT 2005,*, pages 208–216, 2005.

[12] P. M. Niemier, M.T.; Kontz M.J.; Kogge. A design of and design tools for a novel quantum dot based microprocessor. In *Design Automation Conference*, pages 227–232, June 2000.

[13] J. Pearl. *Probabilistic Reasoning in Intelligent Systems: Network of Plausible Inference*. Morgan Kaufmann Publishers, 1998.

[14] G. Toth. *Correlation and Coherence in Quantum-dot Cellular Automata*. PhD thesis, University of Notre Dame, 2000.

[15] P. D. Tougaw and C. S. Lent. Logical devices implemented using quantum cellular automata. *Journal of Applied Physics*, 75(3):1818–1825, Oct 1994.

[16] P. D. Tougaw and C. S. Lent. Dynamic behavior of quantum cellular automata. *Journal of Applied Physics*, 80(15):4722–4736, Oct 1996.

[17] K. Walus, T. Dysart, G. Jullien, and R. Budiman. QCADesigner: A rapid design and simulation tool for quantum-dot cellular automata. *IEEE Trans. on Nanotechnology*, 3(1):26–29, 2004.

X. RESPONSE TO THE REVIEWERS

In this section, we summarize the corrections and modifications made to the original manuscript based on the comments of the Editor and reviewers. First we address the editor's comments and summarize the major revisions. We conclude with detailed responses to the reviewers.

A. Response to the Editor's Comments

The reviewers agree that the paper is well written and well organized and proposes an interesting work. However, they have asked for a number of clarifications and made constructive suggestions. I would ask authors to carefully review the comments, revise the paper and submit it for the second round of review. I look forward to the revised manuscript.

We thank you for compiling all reviews and providing valuable feedback. We address the following issues in the revised manuscript.

1) We added a detailed section on the Bayesian Computing model (section IIIA and III B)

2) We also showed the thermal characteristics of various design implementations of a crosswire in a full adder (section VIII).

3) Defect characterizations of various co-planar crosswires are shown. One important aspect, we observed is that errors in individual devices are often masked at the output. This is not unexpected as logical masking oocuurs also in CMOS. Hence for computational purposes, we have shown that our tool can handle larger circuits. However, it is not possible to make absolute conclusions at circuit level; this aspect of research is beyond the scope of this manuscript. Error masking at the output of a circuit is desirable (as shown in the adder circuit considered in this manuscript) due to the inherent redundancy present in QCA.

B. Response to Reviewers

Next, we address the detailed comments from the reviewers. We thank all reviewers for their valuable time and constructive suggestions.

1) Response to Reviewer 1: In this paper, different coplanar crossing methods in QCA are evaluated using a BN-based simulator in terms of thermal robustness. Among them I find the TMR-based coplanar crossing method especially interesting. Also, the BN simulator provides fast (especially faster than conventional coherence vector and bi-stable engines) and reliable simulation results. Also, evaluation and characterization of single cell defective coplanar crossing circuits described in chapters VI and VII are also useful since the most robust coplanar crossing method can be selected to be used and some other defect tolerant designs can be employed in accordance for the ultimate defect tolerance and thermal robustness. Although the overall quality of this paper is good, I have one suggestion. I recommend the authors to address it in their revised manuscript. Low computational complexity is the primary advantage of the BN simulator used in this paper. There is no doubt about that. However, those coplanar crossing methods evaluated in this paper are not complex QCA circuits. Even the coherence vector model can be used to accurately characterize their thermal and defect robustness. So, I think it will be more interesting and meaningful if the authors to consider a larger circuit design (such as an adder) that contains the number of coplanar crossings to evaluate thermal and defect robustness of the coplanar crossing methods under consideration.

We agree with the reviewer that computational complexity is one of the key advantages of the BN simulator. In the revised manuscript, we have included a new section that details a study of coplanar crossing in a full adder. Few observations are evident as result of this study. First, the thermal performances of individual cross-wires show marginal changes in the polarization as other and relatively less robust QCA components (such as inverters) are already present in the circuit. While characterizing single missing cell defects, again we found that some of the errors in individual designs would be masked at the outputs. Hence relative merits of s is circuit dependent and different possible solutions are possible (as extensively analyzed already

in the literature for CMOS circuits). We have presented the study as well as the observations in a separate section in the revised manuscript.

2) Response to Reviewer 2: It has been shown that even if primitive circuits like a thick crossing works properly and efficiently the system with this kinds of primitive circuits will still very likely malfunction due to sneak noise paths (refer to Kyosun Kim et. al. 's paper on DATE'05), will the thick crossing still be the optimum one from a system perspective? Please justify it.

The effects considered in the referred paper are taken into account also in the proposed solution as the radius of effect is inclusive of the interfering cells in the crossover. The simulation and analysis added for the full adder show that also at a system level the proposed architecture have a positive impact although more limited.

3) Response to Reviewer 3: This is a helpful and timely look at the effect of thermal fluctuations and defects on a specific QCA circuit. The authors imploy a new Bayesian technique that may prove quite useful.

Thank you for encouraging us.

A few points:

(1) The figures are way to small–even for a review copy. It's annoying.

Done

(2) The authors need to be more precise when defining terms. Near the bottom of page 3, the definition of P(xi) is not clear. It would seem to be "the probability of observing the i-th cell to be in state 0".

We have clarified the notation in page 3.

(3) It doesn't do to simply refer to a conference proceeding [2] for the actual method used. The discussion on page 5 fails to state how Equations (2) and (3) are actually used. In particular...

We have added a detailed discussion of the modeling aspects in the two new sections IIIA and IIIB (page 4-page 9) in the revised manuscript.

(4) It is not clear in what sense the circuit is clocked at all. The authors say it is in one clocking zone, but nowhere make clear how the tunneling energy is changed in time. It may be that this is an unclocked calculation.

We are assuming that the crosswires are in a single clocking zone (this can be relaxed to include multiple clocks). Please refer to the newly added section VIII: it shows the crosswires in a full adder design. Also, we have considered the clock energy γ in our simulation.

(5) The tables report an absurd number of significant digits. 2 or 3 at most would be reasonable.

Changed

(6) Similar to (2), in the discussion of single defects the authors are not clear as to what exactly is the situation simulated and what exactly the numbers in Tables III and IV mean?

Tables III and IV are now explained in more detail